Improved YOLOv10 model for detecting surface defects on solar photovoltaic panels

Phat T. Nguyen[1], Loc D. Ho[2], Duy C. Huynh[2]
[1]Department of Circuit theory and measurement, Faculty of Radio-Electronic Engineering, Le Quy Don Technical University,
Ha Noi, Vietnam
[2]HUTECH Institute of Engineering, HUTECH University, Ho Chi Minh City, Vietnam

Article Info	ABSTRACT
	Surface defects greatly affect the performance and service life of photovoltaic (PV) modules. Detecting these defects is important to improve the management, repair and maintenance of PV panels. With the development of artificial intelligence, computer vision brings higher accuracy and lower labor costs than traditional inspection methods. This paper introduces an improved PV you only look once v10 (YOLOv10) model for detecting surface defects of PV modules. The improvement includes adding an exponential moving average (EMA) attention mechanism to the neck, using a cycle generative adversarial network (GAN) to enhance the data, and replacing the YOLOv10 head with a YOLOv9 head to retain non-maximum suppression (NMS). Experiments show that the proposed model outperforms state-of-the-art methods such as YOLOv10s, n, x, b, l, and e, achieving superior detection accuracy. Despite the increased computational cost, the proposed method improved mAP@0.5 and mAP@0.5:0.95 by 5.1% and 6.5% over the original YOLOv10s.

Corresponding Author:

Phat T. Nguyen
Department of Circuit Theory and Measurement, Faculty of Radio-Electronic Engineering, Le Quy Don
Technical University
236 Hoang Quoc Viet Road, Ha Noi, Vietnam
Email: nguyenphat@lqdtu.edu.vn

1. INTRODUCTION

Nowadays, environmental issues and climate change are gaining much attention from individuals, organizations and governments around the world. One of the most important aspects to protect the human environment is the need to reduce greenhouse gas emissions to deal with the problem of global warming. The key, the main driving force of the above task is the need to promote the development of renewable energy, represented by photovoltaic power generation [1]. Numerous statistical findings have confirmed the significance of photovoltaic (PV) systems and grid-connected PV plants worldwide. By the end of 2024, the cumulative installed capacity of solar power systems globally is expected to reach approximately 1.9 TW, up sharply from 1.177 TW at the end of 2022. This increase reflects the explosive growth of solar energy, especially in large markets such as China and the United States [2]. In addition, the installation of PV plants has driven the rapid increase in solar cell deployment globally. For example, in the United States, the cumulative installed capacity of solar power systems is expected to reach approximately 160 GW by the end of 2024 [2]. Meanwhile, in China, the cumulative installed capacity of solar PV systems is forecast to reach approximately 662 GW [2]. However, the power efficiency of photovoltaic cells is frequently constrained by defects that impact both their performance and lifespan. These defects can cause energy loss by forming new

recombination pathways, converting light into heat instead of electricity, or even draining the energy stored in the battery, reducing the efficiency of PV modules [3].

Moreover, emerging generations of solar cells, including copper-indium-gallium-disulfide (CIGS) cells and Perovskite cells (PSCs), are facing challenges in improving energy conversion efficiency, reducing manufacturing costs, and limiting environmental impacts due to the use of toxic materials [4], [5]. Recently, the research and manufacturing industry has paid special attention to PSCs technology due to its simple fabrication process and high conversion efficiency. According to reports from KRICT and MIT, PSCs have achieved an efficiency of 25.2% [5]. However, PSCs still suffer from major problems of low stability, which are affected by factors such as water infiltration, temperature, and humidity conditions, causing chemical and structural changes. This can lead to increased costs and shortened lifespan. Thus, advancing fault detection techniques for predictive maintenance and condition monitoring of PV modules is highly important [5], [6]. There are three methods for detecting defects in PV systems, including image processing-based methods [7]–[10], electrical detection methods [11]–[14], and machine learning-based methods [15]–[24] [25]–[34] [35]. Although image processing and electrical detection methods have achieved quite good results, they lack the ability to adapt to environmental changes, are highly dependent on image quality, and require human intervention to adjust the algorithm. Recently, machine learning has emerged as a potential and effective solution, playing an important role in the development of the PV industry. Deep learning techniques have the potential to greatly enhance detection efficiency, optimize the inspection process at PV power plants, and aid in the operation and maintenance processes. Recent studies on PV defect detection using machine learning techniques are listed in Table 1. Because photovoltaic systems' effectiveness and performance are influenced by various factors, many specific problems are challenging to resolve. However, machine learning techniques can solve these challenges very well, making them popular in defect detection methods.

Table 1. Machine learning models for detecting faults in photovoltaic systems and their outcomes

Ref.	Detection target	Machine learning-method	Results
[15]	Defects in PV cell	Support vector machine (SVM), convolutional neural network (CNN)	Accuracy (CNN): 88.42%; accuracy (SVM): 82.44%
[16]	Tiny cracks and dark spots,	RandomNet50	Accuracy (RandomNet50): 88.23%,
[17]	Defects in PV	CNN	The BER is 7.73% for the binary classification problem.
[18]	Cracks, finger failures	SVM, random forest (RF)	Accuracy (SVM): 99.7%; Accuracy (RF): 96.7%
[19]	Detect defective panels	DeepLabV3+, FPN and U-Net	Accuracy (U-Net): 0.94; Accuracy (FPN): 0.92; Accuracy (DeepLabV3+): 0.87
[20]	Defects in PV	GAN, VGG16	Accuracy (GAN): 0.945; Accuracy (VGG16): 0.96
[21]	Photovoltaic cell defects	Light CNN	93.02% mAP
[22]	Failures in PV modules	SVM	94.4% mAP
[23]	Cracks, oxygen-related defects, defects within cells, and solder disconnections.	ResNet models; YOLO	F1 scores of 0.83 (ResNet18) and 0.78 (YOLO)
[24]	Damaged gate, concealed crack, surface scratch, and hot_spot.	Linear and quadratic discriminant analysis (LDA and QDA)	The QDA algorithm performs better than LDA in the SNR index, enabling it to efficiently detect various defects in PV cells
[25]	Cracked, and heavily busbar-corroded	SVM, RF, and ANN	Accuracy (SVM): 98.77%; Accuracy (RF): 96.6%; Accuracy (ANN): 98.13%;
[26]	Cracked, and corroded	SVM, RF, and CNN	Accuracy (SVM): 99.43%; Accuracy (RF): 97.46%; Accuracy (CNN): 99.71%;
[27]	Without defects, finger interruption, micro-crack, fracture	Proposed CNN	83% mAP
[28]	Cracks, interconnect failures of cells, interruptions in contact, and corrosion of contacts.	Deeplabv3	95.4% mAP
[29]	Cracks (linear and stellate), broken grids, black cores, unaligned, thick lines	ResNet152–Xception	96.17% mAP
[30]	PV fault detection	YOLOv2 and YOLOv3	YOLOv2 achieves an F1 score of 89%, while YOLOv3 reaches 91%
[31]	Faulty area or hot_spot of the PV module.	YOLOv3	34% mAP
[32]	PV fault detection	YOLOv4, YOLOv4-tiny	YOLOv4 has a mAP of 98.8%, whereas YOLOv4-tiny has a mAP of 91.0%.
[33]	PV modules with cracks and fragments	YOLOv5	92.3% mAP
[34]	Hot_spot fault detection	YOLOv5	98.1% mAP
[35]	PV panel defect detection	YOLOv5	97.8% mAP
[36]	PV fault detection	YOLOv8	94% mAP

To enhance the quality and efficiency of detecting defects in photovoltaic systems and support the sustainable advancement of the photovoltaic sector and new energy applications, automating the intelligent defect detection process through advanced computer technology is an essential technical solution. As image analysis and deep learning technologies continue to advance, the integration of computer vision technology with surface defect detection is becoming increasingly prevalent. Currently, machine learning techniques for detecting defects in PV cells are primarily categorized into two types. The first type includes traditional machine learning methods, which depend on manually designed feature extractors to establish complex recognition relationships but often face limitations in terms of generalization and robustness. The second category includes algorithms such as YOLO, region-CNN (R-CNN), MobileNet, InceptionV3, VGG16, and ResNet50, which use deep learning techniques to learn from a large number of samples, providing better generalization and robustness [19]–[21], [27]–[33] [34]–[36]. Among the recently widely used deep learning models with high detection speed and accuracy, the YOLO model, first introduced in 2016 [37], stands out. To overcome the low detection accuracy of the v1 model, YOLOv2 introduced anchor boxes and batch normalization [37]. Building on YOLOv2, YOLOv3 [37] featured a new Darknet architecture with 53 layers, advancing beyond feature pyramid networks to improve multi-scale fusion prediction and accuracy for detecting small and complex objects. YOLOv4 [37] offered a simpler target detection model, reducing the training threshold for the algorithm. YOLOv5 developed five variants (N/S/M/L/X) based on varying channel ratios and model sizes [37]. In late 2022, YOLOv6 and YOLOv7 were released almost simultaneously, with YOLOv6 integrating the RepVGG structure to optimize GPU performance and simplify technical implementation [37]. In January 2023, Ultralytics introduced YOLOv8, which made a major breakthrough in computer vision [37]. YOLOv8 differs from traditional anchor box-based methods by adopting an anchor box-free method by directly predicting the center of the object. YOLOv9, released in February 2024 [37], introduced two major improvements: the programmable gradient information (PGI) framework and the generalized efficient layer pooling network (GELAN). YOLOv10 [37], released in June 2024, demonstrated superior performance over its predecessors. Several case studies [30–36] on PV fault detection using variants of YOLO have demonstrated the richness of models and methods applied to this task. Notably, high accuracy is maintained across a variety of datasets and targets, with metrics such as mAP, AP, and F1. Variants like YOLOv3, YOLOv4, and YOLOv5 often achieve detection accuracy exceeding 98% in certain cases.

The robustness and flexibility of YOLO models in detecting faults in PV systems are highlighted by these results. Therefore, YOLOv10 was improved and used as the main network in this study, which enables fast processing while ensuring high accuracy. The paper also introduces the EMA attention module, which allows the model to extract features efficiently without reducing the detection speed. YOLOv10 is used to detect various types of defects on the surface of photovoltaic panels, including broken, hot_spot, black_border, scratc, and no electricity. Additionally, this paper includes a comparison of YOLOv10 with its earlier versions. The paper's main contributions can be summarized as follows:

a. Improve the neck part of YOLOv10 by integrating the EMA attention mechanism, to enhance the ability to capture the target features.
b. Replace the head part of YOLOv10 with the head part of YOLOv9, because we found that removing non-maximum suppression (NMS) in YOLOv10 does not give good results when dealing with many types of targets with different features, such as on the surface of PV panels, five types of defects.
c. Propose using the cycle-GAN network for data augmentation, although the training time increases, the accuracy of the model has been significantly improved. Data augmentation brings advantages in detecting defects on the surface of PV panels.

The organization of the rest of the paper is as follows: section 2 presents the proposed method, section 3 includes the results and discussion, and section 4 concludes with the findings and future development directions.

2. METHOD
2.1. Original YOLOv10

Developed by researchers at Tsinghua University and based on Ultralytics Python, YOLOv10 introduces a new approach to real-time object detection, aiming to address the limitations of architecture and post-processing found in previous versions of YOLO. The architecture of YOLOv10 is depicted in Figures 1 and 2. The architecture of YOLOv10 inherits the advantages of previous YOLO models while adding important improvements. The structure of the model includes the following main components: Backbone, serving as the feature extractor, YOLOv10 uses an improved version of cross stage partial network (CSPNet) to enhance gradient flow and reduce redundant calculations; The Neck network, designed to aggregate features from multiple levels and transmit them to the head, effectively merges multi-scale features using path aggregation network (PAN) layers. The head part of the YOLOv10 network consists of a one-to-many head and a one-to-one head. The one-to-many head generates multiple expectations for each

object during training to provide rich supervision signals and improve learning accuracy. The one-to-one head only generates the best expectations for each object, eliminating the need for NMS.
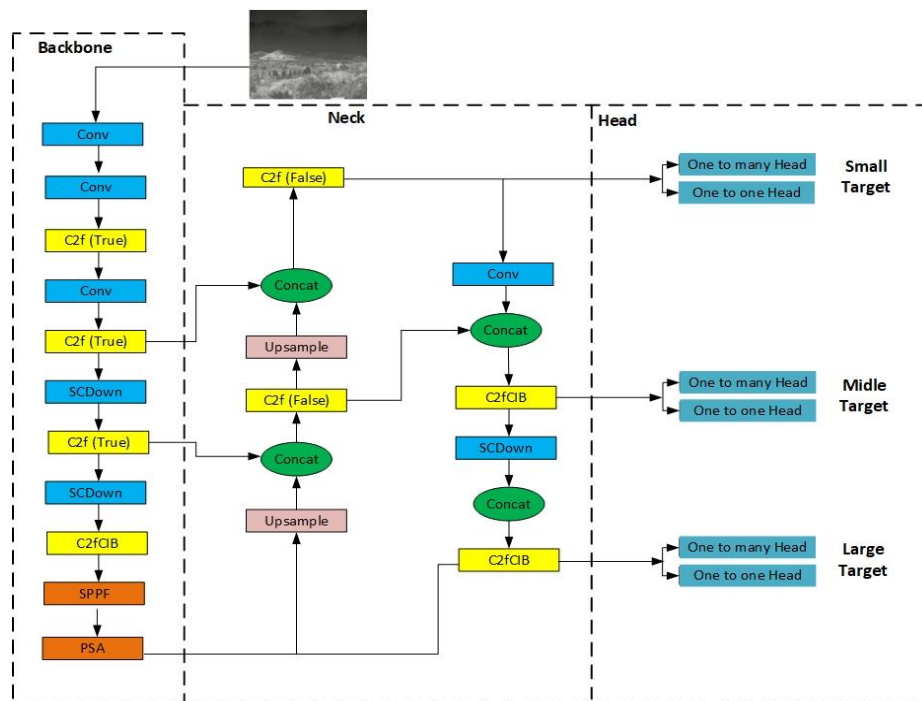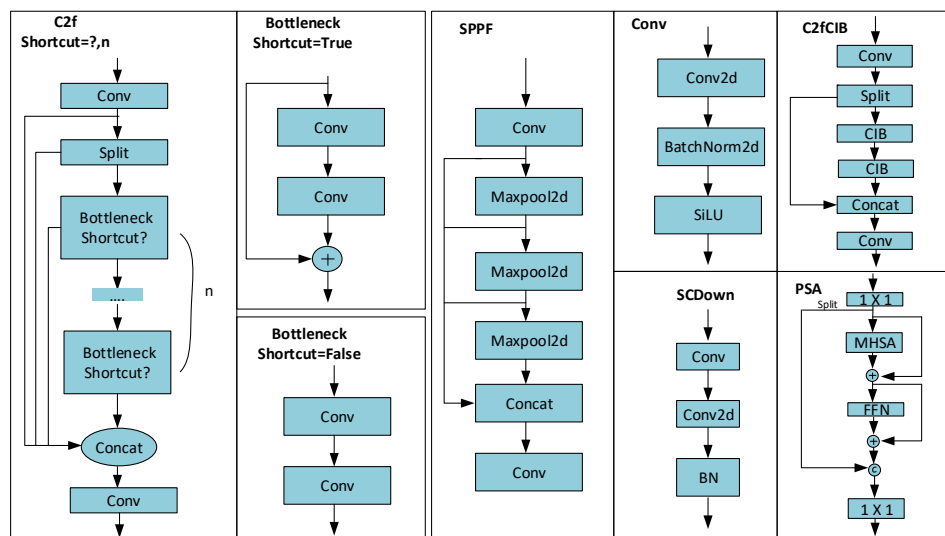

Figure 1. Network structure of YOLOv10 diagram

Figure 2. Diagram of YOLOv10s network detail structure

2.2. Improved YOLOv10

YOLOv10 is the latest version in the YOLO series, marking an important step forward in real-time target detection problems. The YOLOv10 model is highly appreciated for its balance between accuracy and inference time, which is suitable for real-time object detection requirements. However, when applying YOLOv10 to specific problems with special data, adjustments need to be made to make it more suitable. Therefore, this paper improves YOLOv10 to simultaneously detect 5 types of defects on PV and presents the proposed network structure in Figure 3.
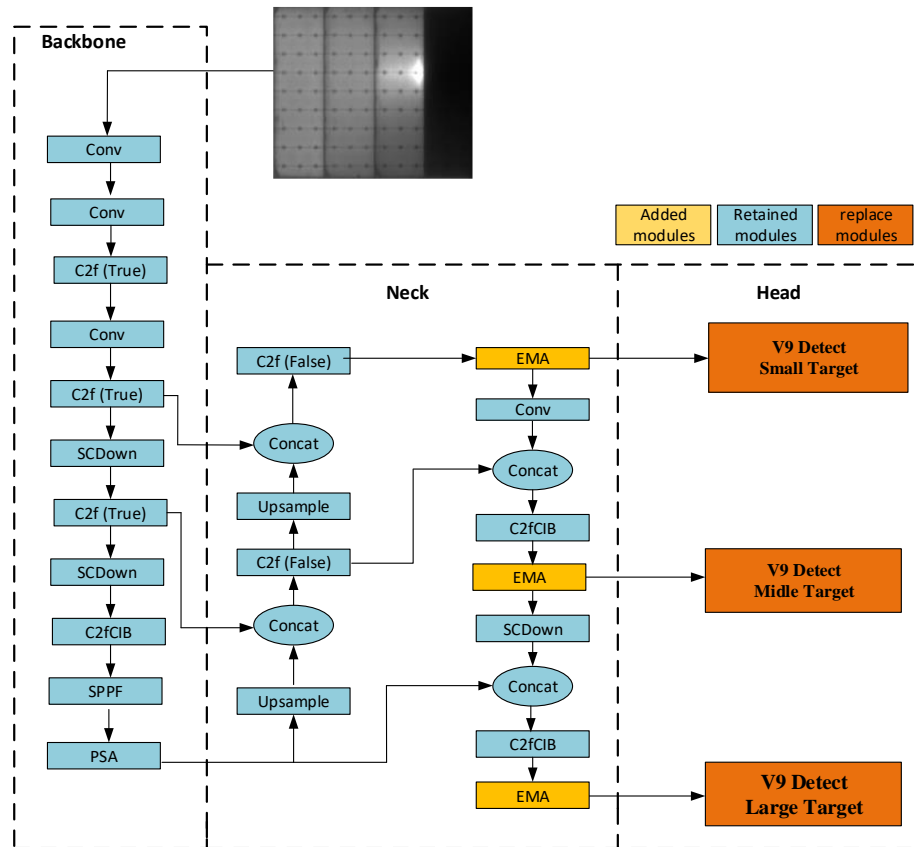
Figure 3. Improved YOLOv10 (PV-YOLOv10) network structure diagram

2.2.1. An improvement of the neck

The neck part of the YOLOv10 network has been extended with a multi-scale attention (EMA) module, as illustrated in Figure 3 [38], [39]. To improve the expressiveness of the PV-YOLOv10 network and construct dependencies, while minimizing the loss of important information between convolutional extractions, the EMA module has been integrated into the neck part of the network. The structure of the EMA is shown in Figure 4. EMA, a parallel attention mechanism commonly applied in computer vision applications, enhances model performance and speeds up processing. In contrast to conventional CNNs, EMA employs a parallel architecture for efficient input data processing. Due to the parallel convolution feature, the model training process becomes faster when working with large data, while improving accuracy by simultaneously processing features at different scales. The key to the effectiveness of EMA lies in the synergistic combination of 3×3 mask and 1×1 branch. Strategically deploying this combination allows for synthesizing multi-scale spatial information, delivering a mechanism for fast and efficient feedback. By flexibly navigating the complex environment of feature extraction, designing ensures strong adaptability to various spatial scales in the data. Comprising two main parallel branches, the EMA architecture includes one branch for performing global clustering in one dimension to encode global information, while the other branch is for extracting features using 3×3 convolution. Modulating and normalizing the outputs from both branches with a sigmoid function, integrating these outputs through a multi-dimensional interaction module captures pixel relationships. Enhancing or weakening the original features by the sigmoid-modulated feature maps leads to a more refined and optimized representation. Consequently, encoding inter-channel information by EMA adjusts the significance of different channels, while maintaining the precise spatial structure details within these channels [39].

2.2.2. An improvement of the head

YOLOv10 introduces a new method called consistent dual labeling for NMS-free training. The NMS-free method allows for a truly end-to-end model implementation, simplifies the inference pipeline, and potentially improves the overall performance of the system. However, since the goal of this paper is to detect defects with similar target characteristics, such as black_border, scratch, and broken, which are quite similar, applying the one-to-many and one-to-one detection heads as in YOLOv10 will likely mis-detect such defects.

For problems that only detect one type of target, the head of YOLOv10 has better performance than previous versions, but for the problem of classifying 5 types of defects as in this paper, the head of YOLOv10 is replaced by the head of YOLOv9 [40] and still uses NMS. Upon identifying and categorizing the faulty areas, NMS is employed to filter the detection boxes, addressing the issue of overlapping target boxes. Determining the IoU value between the detection boxes with the greatest confidence and other detection boxes, as well as examining boxes with IoU values surpassing the designated threshold, is conducted. This procedure continues until only one corresponding detection box remains for each object.
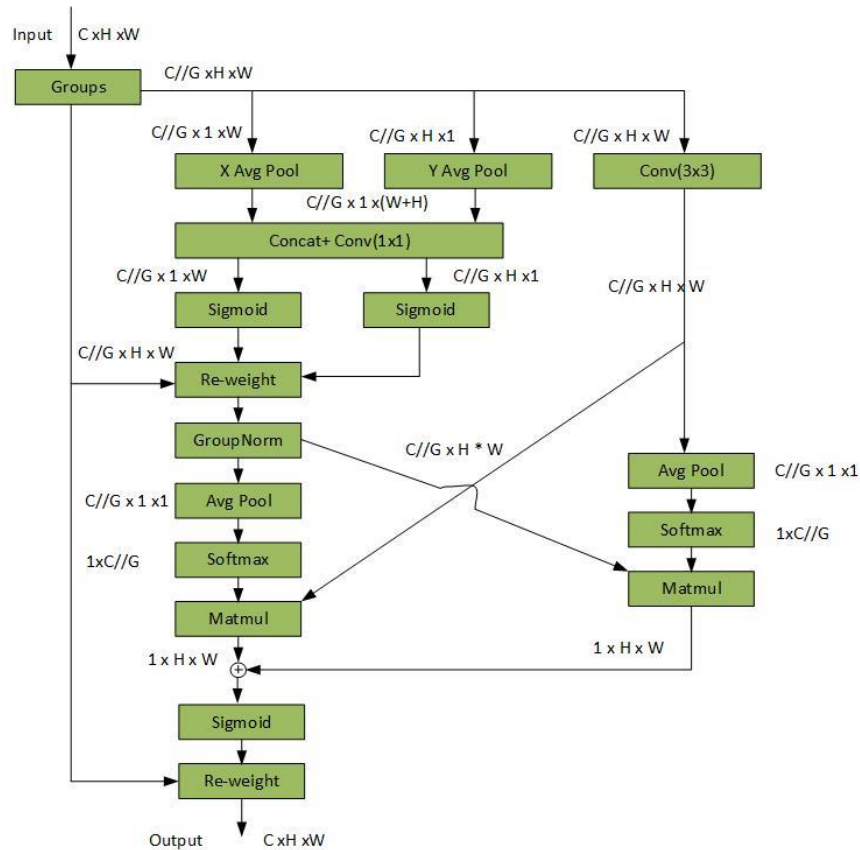

Figure 4. EMA module [38]

2.2.3. Data augmentation using cycle-GAN network

To overcome the problem of limited sample size for deep learning models, a cycle-GAN-based sample enhancement strategy was proposed, in which the error regions are randomly generated to generate pseudo-samples, which helps diversify the existing sample set. In this study, cycle-GAN is applied to generate pseudo-samples from the error regions based on the original data, in order to expand the training dataset, due to the small size of the original dataset and the imbalance between the error classes. The outstanding advantage of cycle-GAN is the ability to train the image transformation model without parallel data pairs [41]. Cycle-GAN, an unsupervised deep learning approach, facilitates bidirectional transformation between the source domain X and the target domain Y, as depicted in Figure 5. It uses two generative networks G1 and G2: G1 transforms from X to Y, and G2 transforms back from Y to X. Both are connected to discriminative networks D1 and D2 after undergoing adversarial training. The networks G and D engage in a competitive process, with D acting as a binary classifier attempting to differentiate between real and fake images, while G aims to deceive D by enhancing the quality of the generated images. Providing an image from the source domain as input to the generative network G, it produces a synthetic image as output. Receiving both the synthetic image and a random image from the target domain, the discriminative network D processes them without requiring pairing. Cycle-GAN was trained for 500 epochs with a fixed learning rate of 0.0002. After this process, the synthetic images are generated by cycle-GAN. In this paper, we created 500 images and their corresponding annotations to enhance the training dataset for the PV-YOLOv10 model.

2.2.4. PV defect detection using PV-YOLOv10 model

The process of detecting surface defects on photovoltaic panels based on the PV-YOLOv10 model, including the steps of data set construction, data augmentation, model training and defect detection, is illustrated in Figure 5. First, the data will be collected, pre-processed, labelled, and then divided into training and testing data sets. The cycle-GAN network is used to augment the training data set. Next, the training parameters are set and the deep learning network is initialized. During this process, the weights of the model are updated through each iteration to ensure the convergence of the loss function, and finally the PV-YOLOv10 model is generated to detect defects on the surface of the panels. The defect detection process is completely automatic, and when a new data set is added, the model configuration parameters can be updated accordingly and re-trained, meeting the actual requirements.
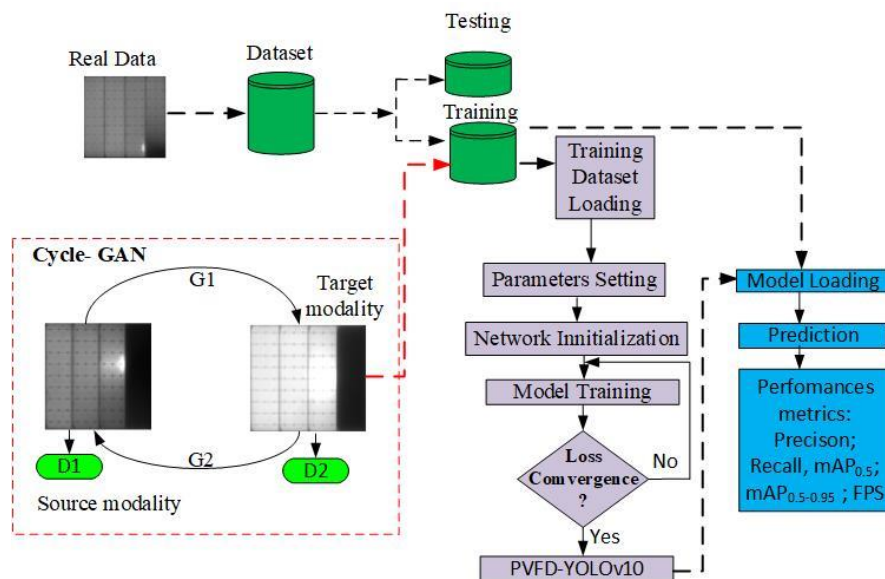

Figure 5. The PV defect detection process based on PV-YOLOv10

3.   EXPERIMENTAL PREPARATION AND RESULTS

3.1. Dataset introduction

We used the public PV multi-defect dataset [35] to validate the effectiveness of our model. This dataset includes five common defect types: broken, hot_spot, black_border, scratch, and no_electricity. Figure 6 illustrates examples of each of these defect types. Images from the PV multi-defect dataset were processed, with a total of 1,108 PV panel surface defect images, divided into 72.8% for the training set and 27.2% for the testing set. Specifically, there are 807 images in the training set and 301 images in the testing set. We used Python to convert the labels from XML to TXT format and serve for model training. There are a total of 4235 defective targets on the 1,108 PV panel surface images. The literature [35] indicates that accounting for the highest proportion of the five defect types, hot_spots constitute 49.09%. Small scratches, representing 36.62%, are followed by black-border targets and broken cells, which account for 6.02% and 3.99%, respectively.
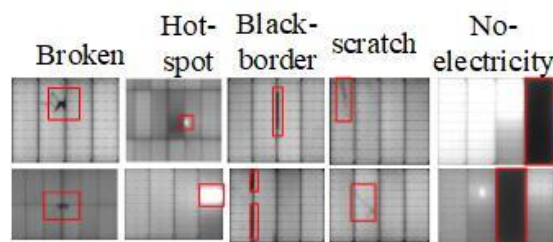

Figure 6. Some samples of 5 types of PV surface defects

3.2. Implementation details

The hardware used for the experiments included a GPU (RTX4070 Ti Super 16 GB), CPU (i5-12600KF), 32 GB RAM, along with PyTorch version 1.13.1 as the deep learning platform and Python version 3.10.13. The dataset was trained over 300 epochs using the Adam optimization algorithm with an initial learning rate of 0.01. The important parameters in the training process are detailed in Table 2.

Table 2. Experimental environment setup

STT	Parameters	Setup
1	Epochs	300
2	Warmup-epochs	3
3	Warmup-momentum	0.8
4	Batch Size	16
5	Imgsize	640×640
6	lrf	0.01
7	lr0	0.01
8	Optimizer	Adam
9	Momentum	0.937

3.3. Evaluation indicators

To evaluate the performance of the proposed model PV-YOLOv10 compared with the newly introduced YOLO versions (YOLOv10s, x, n, m, l), this paper uses statistical indices to compare the models. Throughout the experiment, the evaluations were performed by persistently tuning the parameters. The training and testing sets of the dataset were divided into smaller parts to optimize the model training process so that each index could be tested in detail. As shown in Figure 7, the recall (1), prediction rate (2), and *mAP* graph (4) were verified. The findings indicated that the mAP curve progressively steadied following a specific number of training iterations, while both the recall rate and precision reached the intended outcomes. The *mAP* index represents the average precision per class, while *AP* (3) is the area under the *Pr* (precision-recall) curve, and precision is used to evaluate the performance of the target detection model. The recall rate, or all-test rate, represents the proportion of correctly predicted classes out of the total number of true classes, in contrast to the false detection rate.

$$Re = \frac{TP}{TP+FN} \tag{1}$$

$$Pr = \frac{TP}{TP+FP} \tag{2}$$

where *TP*, *FN*, and *FP* represent the number of true positives, false negatives, and false positives, respectively.

$$AP = \int_0^1 Pr_m(Re_m)dRe_m \tag{3}$$

where Re_m and Pr_m denote the recall and precision for target class *m* and *N* denotes the number of targets. The average precision mean is calculated as (4):

$$mAP = \frac{1}{N}\sum_{i=1}^N AP_i \tag{4}$$

where *N* signifies the number of categories and *AP* stands for the average precision of each category. In the scope of our detection task, $N = 5$.

3.4. Main results

To ensure an accurate representation of the proposed algorithm's detection performance on the dataset detailed in section 3.1, including the background region as a category in the confusion matrix, along with the five defects, was necessary for evaluating the model's effectiveness. In the confusion matrix, representing the true classes of the objects are the rows, while indicating the predicted classes are the columns. Since encompassing all pixels in the image that do not correspond to any defect is the background layer, it is not a class the PV-YOLOv10 model is trained to identify. Thus, when the model is applied to an image, no defect should be classified as belonging to the background layer. Consequently, Figure 8 will show a value of 0 in the background-background column of the PV-YOLOv10 models' confusion matrix,

representing an invalid prediction of the PV-YOLOv10 model. To better understand the values and validation results of the proposed model for detecting five types of PV surface defects, please refer to Table 3. In Table 3, the no_electricity surface defect has the highest mAP value of 0.945, while hot_spot, black_border, broken, and scratch have mAP values of 0.944; 0.932; 0.738; and 0.643, respectively. This primarily results from the fact that the no_electricity defect is large in size and the feature is difficult to confuse, while hot_spot has the largest number of training samples, accounting for nearly half of the total samples. In contrast, scratch and broken are small in size and are easily confused with each other, resulting in relatively low precision, recall, and *mAP* values on scratch and broken.
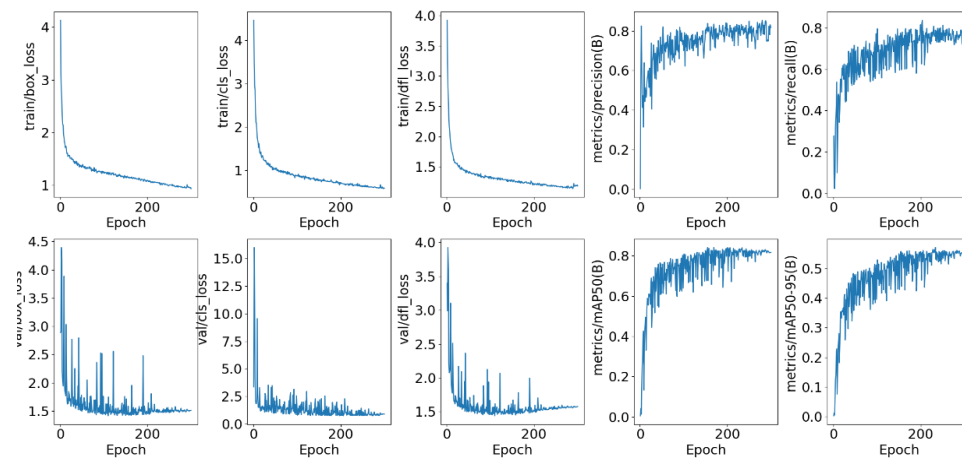

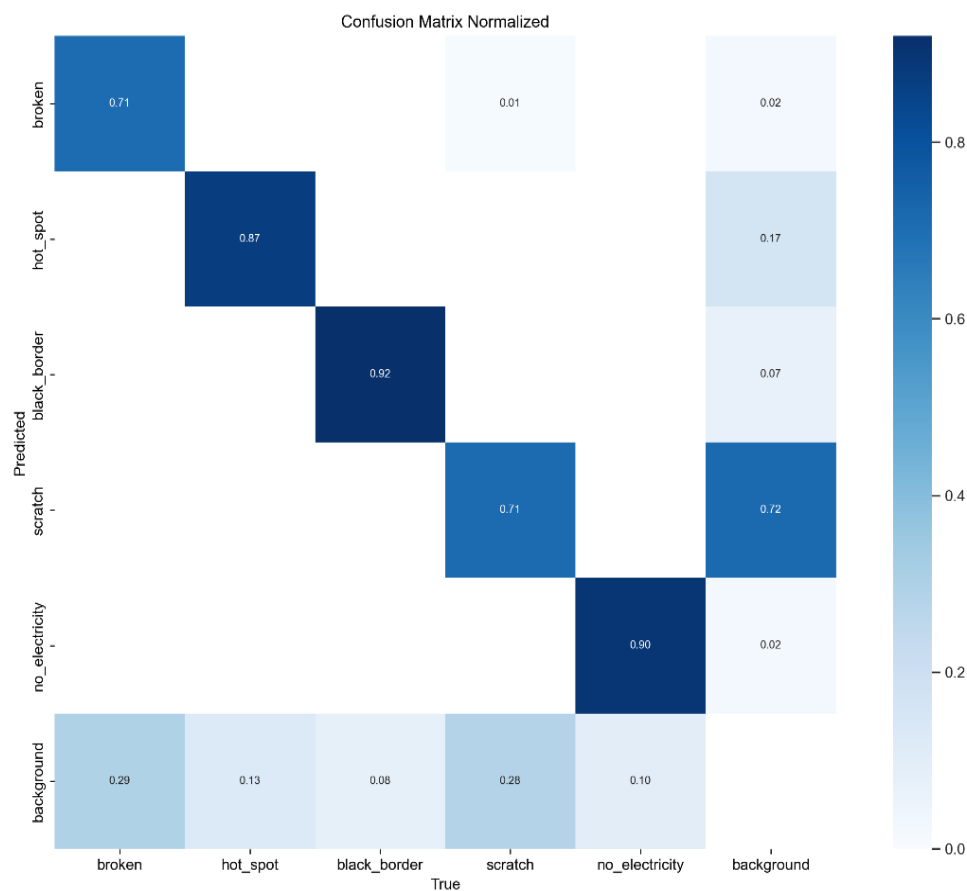Figure 7. PV-YOLOv10 detection index chart

Figure 8. The confusion matrix of PV-YOLOv10 model

Table 3. PV-YOLOv10 detection results

Category	Precision	Recall	*mAP*
broken	0.687	0.706	0.738
hot_spot	0.974	0.808	0.944
black_border	0.809	0.905	0.932
scratch	0.707	0.629	0.643
no_electricity	0.927	0.9	0.945

3.4.1. Ablation experiment

Conducting ablation experiments for a thorough comparison, we aim to verify the effects of different modules on model performance. Starting with the YOLOv10s model as the base, we gradually add additional modules to illustrate the importance of each module and its influence on performance. Showing the results of these experiments, Table 4 demonstrates that achieving the best experimental outcomes requires using all modules, indicating that every module is vital to our strategy.

Improving all model metrics, the addition of the EMA module results in a 0.1% increase in $mAP_{@0.5}$ and a 0.4% rise in $mAP_{@0.5:0.95}$, effectively showcasing its enhancement of the model's feature extraction capabilities. Modifying the head of YOLOv9 resulted in enhancements of 2.5% and 3.1% in $mAP_{@0.5}$ and $mAP_{@0.5:0.95}$, respectively, confirming that this module directs the network to capture more crucial feature information. Integrating both the head modification and the EMA addition led to increases of 4.4% and 3.6% in $mAP_{@0.5}$ and $mAP_{@0.5:0.95}$. Ultimately, employing data augmentation with the Cycle-GAN network elevated mAP@0.5 and $mAP_{@0.5:0.95}$ by 5.1% and 6.5%. The data shown in Table 4 clearly illustrates the essential role and effectiveness of each module, highlighting the advantage of our method.

Table 4. Ablation experiment results

Model	Precision	Recall	$mAP_{@0.5}$	$mAP_{@0.5:0.95}$
YOLOv10s	0.815	0.688	0.789	0.506
YOLOv10s+EMA	0.768	0.717	0.799	0.51
YOLOv10s+Head of YOLOv9	0.801	0.764	0.814	0.537
YOLOv10s+Head of YOLOv9+EMA	0.794	0.787	0.833	0.542
Head of YOLOv9+EMA+GAN (PV-YOLOv10)	0.821	0.79	0.84	0.571

3.4.2. Comparison with state-of-the-art methods YOLOv10

To showcase the superiority of the enhanced PV-YOLOv10 model, this study carried out a series of evaluation experiments, comparing its performance against the newly introduced YOLOv10 models. Offering a concise comparison of various YOLOv10s model versions, Table 5 highlights the architectural diversity among the YOLOv10s variants. These variants, emphasizing different architectural approaches, demonstrate distinct trade-offs between $mAP_{0.5}$; $mAP_{0.5-0.95}$; Precision, recall and GFLOP. The proposed PVDF-YOLOv10 model demonstrates the highest performance in detecting five types of surface defects on PV with $mAP_{0.5}$; $mAP_{0.5-0.95}$; Precision, recall compared to the latest YOLOv10 versions. However, there is a computational trade-off as the GFLOP value of the proposed model is the largest and the most computationally advantageous is the YOLOv10n model with the smallest GFLOP.

Table 5. Results of proposed models PV-YOLOv10 and YOLOv10 versions

Model	$mAP_{@0.5}$	$mAP_{@0.5-0.95}$	Precision	Recall	GFLOP
YOLOv10s	0.789	0.506	0.815	0.688	24.5
YOLOv10m	0.777	0.51	0.756	0.719	63.4
YOLOv10n	0.775	0.513	0.748	0.701	8.2
YOLOv10b	0.803	0.518	0.796	0.74	98
YOLOv10l	0.818	0.533	0.878	0.729	126.4
YOLOv10x	0.821	0.542	0.833	0.763	169.8
PV-YOLOv10	0.84	0.571	0.821	0.79	176.8

3.4.3. Qualitative comparison

To further clarify the effectiveness of the proposed method, we selected some representative images to compare with other state-of-the-art methods. Figure 8 illustrates this specifically. As shown in Figure 9, our model outperforms the YOLOv10n model. Figure 9(a) clearly shows that there are some missed defect detections, marked in red at three different locations with different defect types. Meanwhile, in Figure 9(b), the missed locations in Figure 9(a) were accurately detected by the proposed model. This improvement can

be explained by our model's ability to extract rich semantic features while eliminating the impact of noise. This fully confirms the effectiveness of our method.
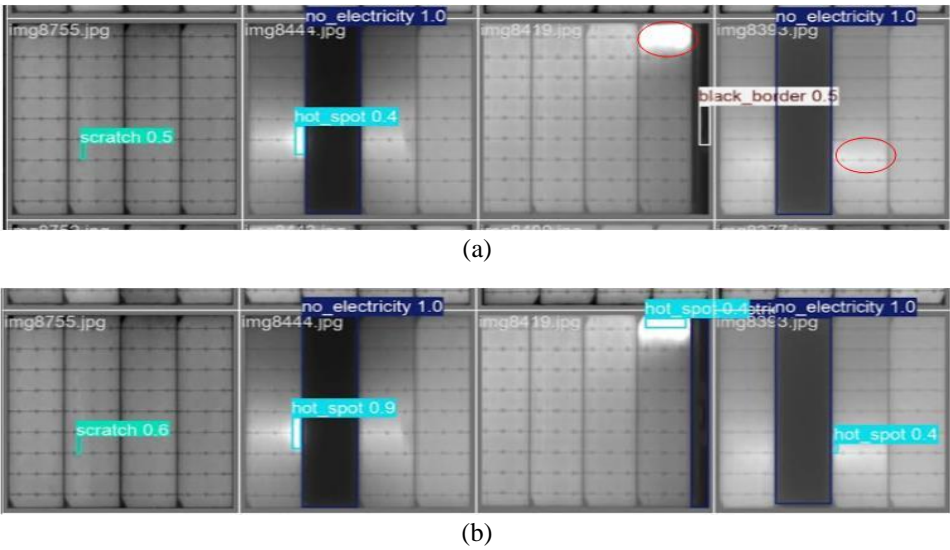

(a)

(b)

Figure 9. Example of (a) YOLOv10n model and (b) PV-YOLOV10 model

4.   CONCLUSION AND OUTLOOK

In this paper, we propose a model named PV-YOLOv10 to detect 5 types of PV panel surface defects. In order to ensure better accuracy on multi-scale defects, the EMA module was introduced to improve the detection phenomenon of small defects, and the head of YOLov10 was replaced by head of YOLOv9 to maintain NMS. In addition, we also used the cycle-GAN method to augment the training data to enhance the training samples, improving the detection performance of the proposed model. Simultaneously, we evaluated our method against the latest state-of-the-art approaches, specifically the YOLOv10 versions, to assess its effectiveness. Enhancing the detection of PV panel surface defects, the proposed model achieved a 5.1% improvement in mAP performance. With the incorporation of additional modules leading to an increase in the number of model parameters and a larger model size, the computational expense rises accordingly. Future research directions could include improving the Backbone part to make the model lighter, or improving the head part of the network to further improve the accuracy of detecting surface defects on PV.

AUTHOR CONTRIBUTIONS STATEMENT

This journal uses the Contributor Roles Taxonomy (CRediT) to recognize individual author contributions, reduce authorship disputes, and facilitate collaboration.

Name of Author	C	M	So	Va	Fo	I	R	D	O	E	Vi	Su	P	Fu
Phat T. Nguyen	✓	✓	✓		✓	✓			✓	✓				
Loc D. Ho					✓			✓			✓			
Duy C. Huynh		✓		✓						✓	✓			

C : **C**onceptualization	I : **I**nvestigation	Vi : **Vi**sualization
M : **M**ethodology	R : **R**esources	Su : **Su**pervision
So : **So**ftware	D : **D**ata Curation	P : **P**roject administration
Va : **Va**lidation	O : Writing - **O**riginal Draft	Fu : **Fu**nding acquisition
Fo : **Fo**rmal analysis	E : Writing - Review & **E**diting	

CONFLICT OF INTEREST STATEMENT
The authors declare no conflict of interest.

DATA AVAILABILITY
The database and code for the findings in this study can be provided by the corresponding author upon reasonable request.

REFERENCES

[1]   C.-C. Ko, C.-Y. Liu, J. Zhou, and Z.-Y. Chen, "Analysis of subsidy strategy for sustainable development of environmental protection policy," *IOP Conference Series: Earth and Environmental Science*, vol. 349, no. 1, p. 012018, Oct. 2019, doi: 10.1088/1755-1315/349/1/012018.

[2]   IEA, "IEA photovoltaic power systems programme," *IEA PVPS*, 2022. https://iea-pvps.org/ (accessed Apr. 15, 2023).

[3]   R. A. Afre and D. Pugliese, "Perovskite solar cells: A review of the latest advances in materials, fabrication techniques, and stability enhancement strategies," *Micromachines*, vol. 15, no. 2, p. 192, Jan. 2024, doi: 10.3390/mi15020192.

[4]   H. Shen *et al.*, "Monolithic perovskite/Si tandem solar cells: pathways to over 30% efficiency," *Advanced Energy Materials*, vol. 10, no. 13, Apr. 2020, doi: 10.1002/aenm.201902840.

[5]   P. Roy, N. Kumar Sinha, S. Tiwari, and A. Khare, "A review on perovskite solar cells: evolution of architecture, fabrication techniques, commercialization issues and status," *Solar Energy*, vol. 198, pp. 665–688, 2020, doi: 10.1016/j.solener.2020.01.080.

[6]   S. Zhang and G. Han, "Intrinsic and environmental stability issues of perovskite photovoltaics," *Progress in Energy*, vol. 2, no. 2, p. 022002, May 2020, doi: 10.1088/2516-1083/ab70d9.

[7]   R. O. Serfa Juan and J. Kim, "Photovoltaic cell defect detection model based on extracted electroluminescence images using SVM classifier," in *2020 International Conference on Artificial Intelligence in Information and Communication (ICAIIC)*, Feb. 2020, pp. 578–582, doi: 10.1109/ICAIIC48513.2020.9065065.

[8]   I. Segovia Ramírez, B. Das, and F. P. García Márquez, "Fault detection and diagnosis in photovoltaic panels by radiometric sensors embedded in unmanned aerial vehicles," *Progress in Photovoltaics: Research and Applications*, vol. 30, no. 3, pp. 240–256, Mar. 2022, doi: 10.1002/pip.3479.

[9]   E. Kaplani, "Detection of degradation effects in field-Aged c-Si solar cells through IR thermography and digital image processing," *International Journal of Photoenergy*, vol. 2012, pp. 1–11, 2012, doi: 10.1155/2012/396792.

[10]   V. Kirubakaran *et al.*, "Infrared thermal images of solar PV panels for fault identification using image processing technique," *International Journal of Photoenergy*, vol. 2022, pp. 1–10, Jun. 2022, doi: 10.1155/2022/6427076.

[11]   S. Vergura, F. Marino, and M. Carpentieri, "Processing infrared image of PV modules for defects classification," in *2015 International Conference on Renewable Energy Research and Applications (ICRERA)*, Nov. 2015, pp. 1337–1341, doi: 10.1109/ICRERA.2015.7418626.

[12]   N. Azkona, A. Llaria, O. Curea, and F. Recart, "Detection, characterization and modeling of localized defects and thermal breakdown in photovoltaic panels from thermal images and IV curves," *Electronic Materials*, vol. 3, no. 2, pp. 154–172, Apr. 2022, doi: 10.3390/electronicmat3020014.

[13]   Varun, M. O. Garg, H. Nautiyal, S. Khurana, and M. K. Shukla, "Heat transfer augmentation using twisted tape inserts: a review," *Renewable and Sustainable Energy Reviews*, vol. 63, pp. 193–225, Sep. 2016, doi: 10.1016/j.rser.2016.04.051.

[14]   M. Alonsogarcia, J. Ruiz, and F. Chenlo, "Experimental study of mismatch and shading effects in the – characteristic of a photovoltaic module," *Solar Energy Materials and Solar Cells*, vol. 90, no. 3, pp. 329–340, Feb. 2006, doi: 10.1016/j.solmat.2005.04.022.

[15]   C. Sun, Y. Li, J. Han, B. Cao, H. Yin, and Y. Shi, "Enhanced photoelectrical properties of alizarin-based natural dye via structure modulation," *Solar Energy*, vol. 185, pp. 315–323, Jun. 2019, doi: 10.1016/j.solener.2019.04.078.

[16]   W. Xu, Y. Shi, R. Yang, B. Ye, and H. Qiang, "Automatic classification of defective solar panels in electroluminescence images based on random connection network," *Electronics*, vol. 13, no. 13, p. 2429, Jun. 2024, doi: 10.3390/electronics13132429.

[17]   A. Bartler, L. Mauch, B. Yang, M. Reuter, and L. Stoicescu, "Automated detection of solar cell defects with deep learning," in *2018 26th European Signal Processing Conference (EUSIPCO)*, Sep. 2018, pp. 2035–2039, doi: 10.23919/EUSIPCO.2018.8553025.

[18]   C. Mantel *et al.*, "Machine learning prediction of defect types for electroluminescence images of photovoltaic panels," *Applications of machine learning*, p. 1, 2019, doi: 10.1117/12.2528440.

[19]   S. Jumaboev, D. Jurakuziev, and M. Lee, "Photovoltaics plant fault detection using deep learning techniques," *Remote Sensing*, vol. 14, no. 15, p. 3728, Aug. 2022, doi: 10.3390/rs14153728.

[20]   F. Lu, R. Niu, Z. Zhang, L. Guo, and J. Chen, "A generative adversarial network-based fault detection approach for photovoltaic panel," *Applied Sciences*, vol. 12, no. 4, p. 1789, Feb. 2022, doi: 10.3390/app12041789.

[21]   M. W. Akram *et al.*, "CNN based automatic detection of photovoltaic cell defects in electroluminescence images," *Energy*, vol. 189, p. 116319, Dec. 2019, doi: 10.1016/j.energy.2019.116319.

[22]   V. S. B. Kurukuru, A. Haque, A. K. Tripathy, and M. A. Khan, "Machine learning framework for photovoltaic module defect detection with infrared images," *International Journal of System Assurance Engineering and Management*, vol. 13, no. 4, pp. 1771–1787, 2022, doi: 10.1007/s13198-021-01544-7.

[23]   X. Chen, T. Karin, and A. Jain, "Automated defect identification in electroluminescence images of solar modules," *Solar Energy*, vol. 242, pp. 20–29, Aug. 2022, doi: 10.1016/j.solener.2022.06.031.

[24]   C. Bu, T. Liu, R. Li, R. Shen, B. Zhao, and Q. Tang, "Electrical pulsed infrared thermography and supervised learning for PV cells defects detection," *Solar Energy Materials and Solar Cells*, vol. 237, 2022, doi: 10.1016/j.solmat.2021.111561.

[25]   J. S. Fada, M. A. Hossain, J. L. Braid, S. Yang, T. J. Peshek, and R. H. French, "Electroluminescent image processing and cell degradation type classification via computer vision and statistical learning methodologies," in *2017 IEEE 44th Photovoltaic Specialist Conference (PVSC)*, Jun. 2017, pp. 3456–3461, doi: 10.1109/PVSC.2017.8366291.

[26]   A. M. Karimi *et al.*, "Automated pipeline for photovoltaic module electroluminescence image processing and degradation feature classification," *IEEE Journal of Photovoltaics*, vol. 9, no. 5, pp. 1324–1335, Sep. 2019, doi: 10.1109/JPHOTOV.2019.2920732.

[27]   W. Tang, Q. Yang, K. Xiong, and W. Yan, "Deep learning based automatic defect identification of photovoltaic module using electroluminescence images," *Solar Energy*, vol. 201, pp. 453–460, May 2020, doi: 10.1016/j.solener.2020.03.049.

[28]   J. Fioresi *et al.*, "Automated defect detection and localization in photovoltaic cells using semantic segmentation of electroluminescence images," *IEEE Journal of Photovoltaics*, vol. 12, no. 1, pp. 53–61, 2022, doi: 10.1109/JPHOTOV.2021.3131059.

[29] J. Wang *et al.*, "Deep-learning-based automatic detection of photovoltaic cell defects in electroluminescence images," *Sensors*, vol. 23, no. 1, p. 297, Dec. 2022, doi: 10.3390/s23010297.

[30] A. Greco, C. Pironti, A. Saggese, M. Vento, and V. Vigilante, "A deep learning based approach for detecting panels in photovoltaic plants," in *Proceedings of the 3rd International Conference on Applications of Intelligent Systems*, Jan. 2020, pp. 1–7, doi: 10.1145/3378184.3378185.

[31] S. P. Pathak, D. S. Patil, and S. Patel, "Solar panel hotspot localization and fault classification using deep learning approach," *Procedia Computer Science*, vol. 204, pp. 698–705, 2022, doi: 10.1016/j.procs.2022.08.084.

[32] A. Binomairah *et al.*, "Detection of microcracks and dark spots in monocrystalline PERC cells using photoluminescene imaging and YOLO-based CNN with spatial pyramid pooling," *EPJ Photovoltaics*, vol. 13, 2022, doi: 10.1051/epjpv/2022025.

[33] S. Xu, H. Qian, W. Shen, F. Wang, X. Liu, and Z. Xu, "Defect detection for PV modules based on the improved YOLOv5s," in *Proceedings - 2022 Chinese Automation Congress, CAC 2022*, 2022, vol. 2022-Janua, pp. 1431–1436, doi: 10.1109/CAC57257.2022.10055183.

[34] Q. Zheng, J. Ma, M. Liu, Y. Liu, Y. Li, and G. Shi, "Lightweight hot-spot fault detection model of photovoltaic panels in UAV remote-sensing image," *Sensors*, vol. 22, no. 12, p. 4617, Jun. 2022, doi: 10.3390/s22124617.

[35] L. Li, Z. Wang, and T. Zhang, "GBH-YOLOv5: Ghost convolution with BottleneckCSP and tiny target prediction head incorporating YOLOv5 for PV panel defect detection," *Electronics*, vol. 12, no. 3, p. 561, Jan. 2023, doi: 10.3390/electronics12030561.

[36] Q. B. Phan and T. T. Nguyen, "A novel approach for PV cell fault detection using YOLOv8 and particle swarm optimization," in *2023 IEEE 66th International Midwest Symposium on Circuits and Systems (MWSCAS)*, Aug. 2023, pp. 634–638, doi: 10.1109/MWSCAS57524.2023.10406139.

[37] C.-Y. Wang and H.-Y. M. Liao, "YOLOv1 to YOLOv10: the fastest and most accurate real-time object detection systems," *APSIPA Transactions on Signal and Information Processing*, 2024, doi: 10.1561/116.20240058.

[38] D. Ouyang *et al.*, "Efficient multi-scale attention module with cross-spatial learning," in *ICASSP 2023 - 2023 IEEE International Conference on Acoustics, Speech and Signal Processing (ICASSP)*, Jun. 2023, pp. 1–5, doi: 10.1109/ICASSP49357.2023.10096516.

[39] J. Zhu, T. Hu, L. Zheng, N. Zhou, H. Ge, and Z. Hong, "YOLOv8-C2f-faster-EMA: an improved underwater trash detection model based on YOLOv8," *Sensors*, vol. 24, no. 8, p. 2483, Apr. 2024, doi: 10.3390/s24082483.

[40] C.-Y. Wang, I.-H. Yeh, and H.-Y. Mark Liao, "OLOv9: Learning what you want to learn using programmable gradient information," 2025, pp. 1–21, doi: 10.1007/978-3-031-72751-1_1.

[41] M. Hammami, D. Friboulet, and R. Kechichian, "Cycle GAN-based data augmentation for multi-organ detection in CT images via YOLO," in *2020 IEEE International Conference on Image Processing (ICIP)*, Oct. 2020, pp. 390–393, doi: 10.1109/ICIP40778.2020.9191127.

BIOGRAPHIES OF AUTHORS

Phat T. Nguyen ⓘ � Education and research: He received the M.E, and the Ph.D. degrees in electrical engineering from Ryazan State Radio-Engineering University, Russia, in 2012 and 2015, respectively. Current job summary: he is a senior lecturer, Le Quy Don Technical University. His field of interest: application of artificial intelligence in the fields of signal processing, image processing, remote sensing, renewable energy power systems. He can be contacted at email: nguyenphat@lqdtu.edu.vn.

Loc D. Ho ⓘ � received the B.Sc. degree in electrical engineering from the National Technical University, Kharkiv Polytechnic Institute, Ukraine, in 1991, the D.Eng. degree in automation engineering from the Igor Sikorsky Kyiv Polytechnic Institute, National Technical University of Ukraine, Ukraine, in 1994, and the Dr. Sc. degree in automation engineering from the National Research University, Moscow Power Engineering Institute, Russia, in 2002. He is currently a Professor and the President of the HUTECH University, Vietnam. His research interests include control and operation in power systems, microgrids, and smart grids; stability analysis in control systems; soft computing techniques such as neural networks, and fuzzy logics; meta-heuristic algorithms such as genetic algorithms, and particle swarm optimization algorithms; and cloud computing techniques. He can be contacted at email: hdloc@hutech.edu.vn.

Duy C. Huynh ⓘ � (Senior Member, IEEE) received the B.E. and M.E. degrees in electrical engineering from the University of Technology, Vietnam National University of Ho Chi Minh City, Vietnam, in 2001 and 2005, respectively, and the Ph.D. degree in electrical engineering from Heriot-Watt University, Edinburgh, U.K., in 2010. He is currently an associate professor of electrical engineering. His research interests include the areas of energy-efficient control and parameter estimation for induction machine drive systems, power systems, renewable energy systems, microgrids, and smart grids. He can be contacted at email: hc.duy@hutech.edu.vn.